Korean J. Chem. Eng., 40(7), 1783-1791 (2023)
DOI: 10.1007/s11814-023-1432-0

pISSN: 0256-1115
eISSN: 1975-7220

Effect of Cr_2O_3 on the viscosity and structure of slag (or glass) of CaO-MgO-Al_2O_3-SiO_2 system

Yifan Wang, Yici Wang†, Yunhao Zhang, Yifan Chai, Fengguang Zhao, and Guoping Luo

School of Materials and Metallurgy, Inner Mongolia University of Science and Technology, Baotou 014010, China
(*Received 13 August 2022 • Revised 16 January 2023 • Accepted 3 February 2023*)

Abstract−The glass-ceramics of CaO-MgO-Al_2O_3-SiO_2-Cr_2O_3 system was prepared by melting method using blast furnace slag, low-carbon ferrochrome alloy slag and quartz sand as raw materials, and the effect of Cr_2O_3 on the viscosity and structure of slag (or glass) of CaO-MgO-Al_2O_3-SiO_2 (CMAS) system at high temperature was studied. The Urbain viscosity prediction model was established and optimized, and the effect of Cr_2O_3 on the structure of slag (or glass) was studied by Raman spectroscopy. The results show that when the mass fraction of Cr_2O_3 is in the range of 0.85-2.05%, the viscosity of slag (or glass) of CMAS system decreases with the increase of Cr_2O_3 content. The average relative errors between the experimented viscosity value and the calculated viscosity value obtained by using the optimized Urbain model are less than 20%, which is effective and universal for the viscosity prediction of slag (or glass) of CaO-MgO-Al_2O_3-SiO_2-Cr_2O_3 system. With the increase of Cr_2O_3 content, the complex silicon oxygen tetrahedrons (Q_3) disintegrate into a larger number of simple silicon oxygen tetrahedrons (Q_0, Q_1, Q_2), resulting in the sparse structure of the melt network and a decrease in macroscopic viscosity.

Keywords: Cr_2O_3, Viscosity, Glass-ceramics, Urbain Model, Raman Spectroscopy, Tetrahedron Silica

INTRODUCTION

With the development of the metallurgical industry, the emission of metallurgical slag harmful to the environment has increased year by year, and most of the harmful metallurgical slag is disposed of by landfill, microbial treatment and other methods [1]. Studies have shown that a variety of metallurgical slags can be used to prepare glass-ceramics [2,3], which provides a new way for the utilization of metallurgical slag. Glass-ceramics is a new type of material with high mechanical strength, chemical corrosion resistance and other advantages, and glass-ceramics with slag as raw material is mainly used as a building decoration material [4]. Blast furnace slag and low-carbon ferrochrome alloy slag are industrial solid wastes discharged by the metallurgical industry, the main components of both are CaO, MgO, Al_2O_3 and SiO_2, and the low-carbon ferrochrome alloy slag contains the nucleation agent component Cr_2O_3 that can promote crystallization of glass-ceramics [5,6], so the blast furnace slag and low-carbon ferrochrome alloy slag are suitable for the preparation of glass-ceramics for architectural decoration of CaO-MgO-Al_2O_3-SiO_2-Cr_2O_3 system [7].

Viscosity is one of the important physical properties when preparing glass-ceramics by melting method, which runs through the melting and forming stages of glass production, which greatly affects the mass transfer of elements in the melt and the performance of glass [8], and has a great impact on the preparation process and product quality of glass-ceramics. It takes a considerable amount of time and money to measure the viscosity of slag (or glass) under high temperature conditions, and it is unrealistic to obtain the viscosity value of slag (or glass) only from experimental means, so it is necessary to establish a reliable model to predict the viscosity of the slag (or glass), so as to provide accurate information for the preparation of glass-ceramics. The Urbain model has achieved good results in the viscosity prediction of conventional CMAS system slag and its subsystems, and has a wide range of applications [9]. For example, Dong et al. modified the Urbain model and applied it to predict the slag viscosity of TiO_2-Al_2O_3-CaO-SiO_2 and TiO_2-Al_2O_3-CaO-MgO-SiO_2 systems, with good prediction results [10]. At present, the study on the use of Urbain model to predict the viscosity of slag (or glass) of CaO-MgO-Al_2O_3-SiO_2 system containing Cr_2O_3 has not yet been reported in the literature. This study is based on a previous study of Urbain model, combined with the viscosity data measured experimentally; the Urbain model parameters were optimized to predict the viscosity of slag (or glass) of CMAS system containing Cr_2O_3. In addition, Raman spectroscopy was used to analyze the influence of Cr_2O_3 on the melt structure of CMAS system, which provided a scientific basis for the rational use of chromium-containing slag to prepare CMAS glass-ceramics.

MATERIALS AND METHODS

1. Determination of the Composition of the Glass-ceramics

The blast furnace slag used in this study was taken from the Baotou Iron and Steel Works, and the low-carbon ferrochrome alloy slag was from a chromium ferroalloy plant in Inner Mongolia, with quartz sand as a conditioning agent [11,12]. X-ray fluorescence analysis was used to determine the chemical composition of each raw material as shown in Table 1.

From Table 1, it can be seen that the sum of the mass percentage

†To whom correspondence should be addressed.
E-mail: wangyici01060@163.com

Table 1. The chemical composition of raw materials (mass fraction, %)

Component	CaO	SiO_2	Al_2O_3	MgO	CaF_2	CaS	MnO
Blast furnace slag	34.43	34.21	13.84	9.15	0.78	3.2	0.52
Chromium iron alloy slag	48.64	29.46	7.36	7.23	-	-	-
Quartz sand	0.029	98.200	0.120	0.005	-	-	-
Component	Fe_2O_3	FeO	K_2O	Na_2O	Cr_2O_3	TiO_2	Other
Blast furnace slag	-	0.69	0.48	0.54	-	0.89	1.27
Chromium iron alloy slag	0.58	0.5	-	-	3.48	-	2.75
Quartz sand	0.037	-	-	0.018	-	-	1.591

of the main components CaO, SiO_2, Al_2O_3 and MgO in the blast furnace slag of Baotou Iron and Steel Works is as high as 91.63%, and a small number of components K_2O and Na_2O can reduce the melting point of glass [13], so the blast furnace slag of Baotou Iron and Steel Works is an ideal raw material for the preparation of CMAS system glass-ceramics. CaO, SiO_2, MgO and Al_2O_3 in the low-carbon ferrochrome alloy slag account for 92.69% of the total mass percentage of the slag, and the nucleation agent Cr_2O_3 is 3.48%, so the low-carbon ferrochrome alloy slag is also an ideal raw material for the preparation of CMAS system glass-ceramics. Therefore, it is completely feasible to adjust the content of the nucleation agent Cr_2O_3 by adjusting the ratio of blast furnace slag and low-carbon ferrochrome alloy slag, and to prepare glass-ceramics with quartz sand as a supplementary silicon source.

Glass-ceramic with pyroxene as the main crystalline phase has excellent physical and chemical properties. Therefore, based on the ternary phase diagram of CaO-Al_2O_3-SiO_2 with MgO mass fraction of 5% drawn by using Factsage software (see Fig. 1), six adjacent base glass composition points were selected in the pyroxene region (black area). By changing the ratio of blast furnace slag and low-carbon ferrochrome alloy slag, and adjusting the amount of quartz sand, the mass fraction of Cr_2O_3 in each group of raw materials was 0.85%, 1.11%, 1.36%, 1.60%, 1.83% and 2.05%, respectively. The chemical composition of six groups of glass-ceramics is shown in Table 2.

The viscosity of slag (or glass) is mainly affected by temperature, basicity and Cr_2O_3 content [14,15]. From Table 2, it can be seen that the main chemical composition of glass-ceramics is 31%-34%CaO, 45%-49%SiO_2, 6%-10%Al_2O_3, 5%-7%MgO and 0.85%-2.05%Cr_2O_3. In this study, the binary basicity value and quaternary basicity value

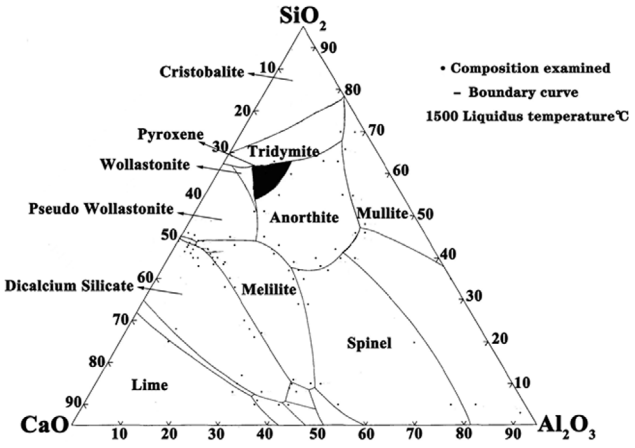

Fig. 1. CaO-Al_2O_3-SiO_2 ternary phase diagram with 5% MgO.

of slag (or glass) were kept constant, which was 0.7. Therefore, when the temperature was fixed, the Cr_2O_3 content was the main factor affecting the viscosity of the slag (or glass), which laid a foundation for exploring the influence of Cr_2O_3 on the viscosity of the slag (or glass) of the CMAS system.

In addition, the value of the acidity coefficient reflects whether the designed raw materials ratio can be made of glass [16]. Acidity coefficient refers to the ratio of the amount of acidic oxide and alkaline oxide in the materials, for CMAS system slag (or glass), a reasonable acidity coefficient range is 1.00-1.30. According to the chemical composition of the raw materials, the acidity coefficient of the six groups of samples was calculated to be in the range of 1.03-1.09, as shown in Table 2. All of them were within the rea-

Table 2. Chemical composition of glass-ceramics (mass fraction, %)

Composition / Numbering	CaO	SiO_2	Al_2O_3	MgO	Cr_2O_3	Other	Binary basicity	Quaternary basicity	Acidity coefficient
S1	31.40	45.46	9.65	6.96	0.85	5.68	0.7	0.7	1.03
S2	31.90	46.18	8.94	6.67	1.11	5.20	0.7	0.7	1.05
S3	32.38	46.85	8.26	6.39	1.36	4.76	0.7	0.7	1.06
S4	32.85	47.51	7.61	6.12	1.60	4.31	0.7	0.7	1.07
S5	33.30	48.14	6.98	5.86	1.83	3.89	0.7	0.7	1.08
S6	33.67	48.67	6.53	5.60	2.05	3.48	0.7	0.7	1.09

Note: Binary basicity=ω(CaO)/ω(SiO_2), quaternary basicity=ω(CaO+MgO)/ω(SiO_2+Al_2O_3).

Table 3. Comparison of viscosity models

Model	Model core features	Characteristics	Application
Urbain	Based on Frenkel-Weymann liquid viscosity model	There are different model parameters for different slag systems and the same set of parameters cannot be applied to all slag systems.	CaO, MgO, Al_2O_3, SiO_2, Cr_2O_3, B_2O_3, MnO, FeO, PbO
Iida et al.	Related to slag basicity	It can be used to predict the viscosity of blast furnace slag well, but only for a few simple systems.	CaO, MgO, Al_2O_3, SiO_2
Riboud et al.	Based on Frenkel-Weymann viscosity model	The prediction results of slag system containing K_2O and Na_2O are good, but the applicable temperature and composition range are narrow.	CaO, MgO, Al_2O_3, SiO_2, K_2O, Na_2O
NPL	Related to the optical basicity of molten slag	It can get certain prediction effect for slag system without Fe, but there is a large positive deviation.	CaO, MgO, Al_2O_3, SiO_2, TiO_2, B_2O_3, MnO, FeO, BaO, Li_2O
Quasi-chemical	Related to slag structure	The calculation is too complicated and the corresponding model parameters are not given.	CaO, MgO, Al_2O_3, SiO_2, FeO
KTH	Based on absolute rate	The viscosity is related to the Gibbs free energy of thermodynamics, but the calculation is too complicated.	CaO, MgO, Al_2O_3, SiO_2

sonable range of the prepared glass, so the ratio of raw materials was reasonable and feasible.

2. Experimental

2-1. Viscosity Measurement and Raman Spectrum Measurement

The viscosity of the slag (or glass) was determined by the inner cylinder rotation method [17], and the instrument used the RTW-10 melt physical properties comprehensive analyzer, PtRh10-Pt thermocouple was used for temperature measurement, and the furnace was N_2 atmosphere. The fully mixed 150 g sample was loaded into a graphite crucible, placed in the constant temperature zone of the electric furnace to heat up and melt, the furnace temperature rose to 1,500 °C to keep warm for 30 min, and then the slag (or glass) viscosity was determined at a cooling rate of 4 °C/min; the test was stopped when it reached 3 Pa·s. Raman spectrum analysis was carried out after water quenching of slag in molten state. HORIBA HR Evolution high resolution Raman spectrometer was used as the instrument, and the 532 nm solid-state laser was used as the light source, and the measured frequency range was 800-1,200 cm^{-1}.

2-2. Comparison of Viscosity Models

For a long time, some scholars have established many viscosity models for CaO-MgO-Al_2O_3-SiO_2 quaternary slag system, which can effectively predict the viscosity of slag in a certain range of slag temperature and composition. These models can be mainly divided into two categories: one is empirical model, such as Urbain model, Iida model, Riboud model and NPL model [18-21]. This kind of model is based on mathematical formulas and fitting experimental data to obtain model parameters for viscosity prediction. The other is a structural model, such as quasi-chemical model and KTH model. In this type of model, there are many parameters and the derivation and calculation process are complicated, which requires the help of professional calculation software. The comparison of these different viscosity models is shown in Table 3.

According to Table 3, among the various viscosity models, the Iida model and Riboud model have a narrow prediction range and are not suitable for slag containing Cr_2O_3, the optical basicity studied by the NPL model is inconsistent with the study in this paper, as the calculation of the quasi-chemical model and KTH model is too complex. Urbain model has a good viscosity prediction effect for the conventional CaO, MgO, Al_2O_3, SiO_2 quaternary system and its sub-systems. Therefore, Urbain model was selected to predict the viscosity of CaO-MgO-Al_2O_3-SiO_2-Cr_2O_3 slag (or glass) system discussed in this study.

2-3. Raman Spectroscopy

Raman spectroscopy is an analytical method applied to the study of molecular structure [22], the most basic unit in the silicate melt structure is the silicon oxygen tetrahedron, where the oxygen (Si-O_b-Si) connected to two Si at the same time is the bridge oxygen, and the oxygen (Si-O_{nb}-M) connected to one Si and one metal cation is the non-bridge oxygen [23]. According to the different number of bridge oxygen in the same silicon oxygen tetrahedron, the structural units in the silicate molecular network are defined as five different silicon oxygen tetrahedrons Q_n (Q stands for silicon oxygen tetrahedron, n represents the number of bridge oxygen in the tetrahedron, the value is 0, 1, 2, 3, 4), and these Q_n have their own characteristic lines in the Raman spectrum [24]. Among them, the Raman displacement zone corresponding to Q_n in the melt of CaO-MgO-Al_2O_3-SiO_2-Cr_2O_3 system is shown in Table 4.

2-4. Preparation of Water Quenched Samples

Before using Raman spectroscopy to analyze the molten slag after water quenching (mainly the vitreous body), it is necessary to determine its amorphous properties [25], and the water quenching slag can retain the structural information of the melt state, so the study of the melt structure requires water quenching treatment of the molten slag. The mixed raw materials were placed in the corundum cru-

Table 4. The Raman shift region corresponding to Q_n (n=0-4) line

Q_n	Raman shift region (cm^{-1})
Q_0	850-880
Q_1	900-930
Q_2	950-1,000
Q_3	1,040-1,060
Q_4	1,200

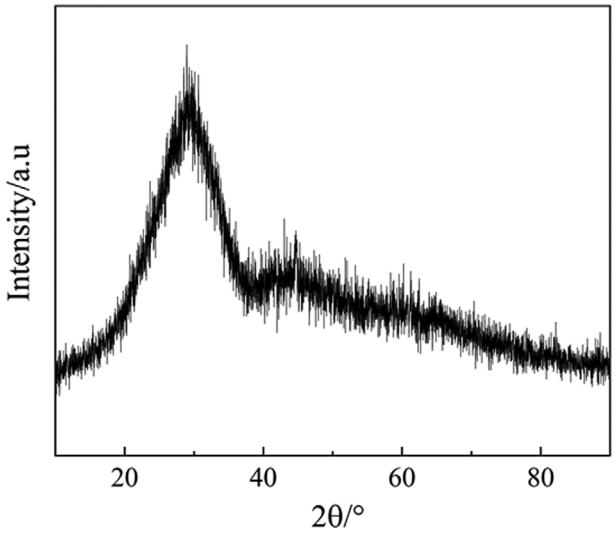

Fig. 2. XRD test result of water quenched sample.

cible and placed in the $MoSi_2$ high-temperature electric furnace, heated to 1,460 °C under an air atmosphere, and held for 3 h to make the melt structure uniform, after the heat preservation, the molten slag in the corundum crucible was quickly poured into water to cool to obtain a water quenching sample. The water-quenched sample was crushed below 200 mesh and tested using XRD. The XRD test result is shown in Fig. 2, where there is no significant crystallization peak, indicating that the sample is amorphous. Subsequently, six groups of water-quenched samples were tested by Raman spectroscopy.

RESULTS AND DISCUSSION

1. Urbain Model Optimization

Fig. 3 shows the viscosity-temperature (η-T) data curves of six sets of slag (or glass), indicating that in the range of 1,300-1,460 °C, when the basicity is unchanged, the increase in Cr_2O_3 content leads to a decrease in the viscosity of the slag macroscopically. In this study, at the glass melting temperature of 1,460 °C, the viscosity of molten slag (or glass) measured ranged from 0.547 Pa·s to 0.694 Pa·s (see Fig. 3), and the melt fluidity was good. With the increase of Cr_2O_3 content, the amount of magnesium-chromium spinel formed by Cr_2O_3 and MgO in the melt should have increased [26], but the glass viscosity showed a downward trend. The results indicate that magnesium-chromium spinel does not exist or exists in small amounts, but it has little effect on melt viscosity. This point can be confirmed by XRD test result of glass phase after rapid cooling of melt (see Fig. 2). No magnesium-chromium spinel phase is found in the XRD images, so the slag (or glass) melt is considered to be a Newtonian fluid with low viscosity.

Building a mathematical model from several sets of measured η-T data can be used to predict the viscosity of slag (or glass) of $CaO\text{-}MgO\text{-}Al_2O_3\text{-}SiO_2\text{-}Cr_2O_3$ systems, saving time and money, and is of great significance for improving the efficiency of glass-ceramics preparation. The Urbain model is based on the Weymann-Frenkel equation [27], whose η-T relation is as follows [28]:

$$\eta = AT\exp(1{,}000B/T) \tag{1}$$

$$-\ln A = mB + n \tag{2}$$

where η is the viscosity (Pa·s), T is the absolute temperature (K), A is the pre-index factor, B is viscous activation energy, m and n are both pending constants that can be determined experimentally.

The Urbain model has different pending constants m, n for different systems [29], so it is necessary to determine the m and n values applicable to the $CaO\text{-}SiO_2\text{-}MgO\text{-}Al_2O_3\text{-}Cr_2O_3$ five-element system to predict the viscosity of the slag (or glass) system. First, the pending constants m and n in the Urbain model were determined from the η-T data of the experiment [30].

For each sample, its η-T satisfied formula (1) η=ATexp(1,000B/T). Dividing both sides of the formula by T, and $\ln\frac{\eta}{T} = B\frac{1{,}000}{T} + \ln A$ can be obtained by logarithm. Take $\frac{1{,}000}{T}$ as abscissa and $\ln\frac{\eta}{T}$ as ordinate, makes $\ln\frac{\eta}{T} - \frac{1{,}000}{T}$ the relation curve, and obtains the

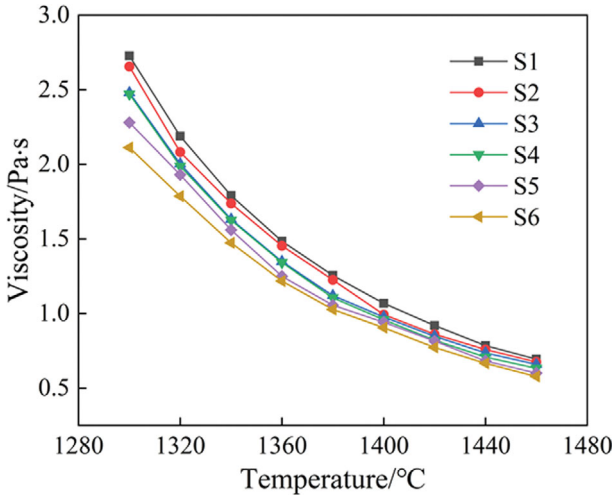

Fig. 3. "η-T" curves of six groups of samples.

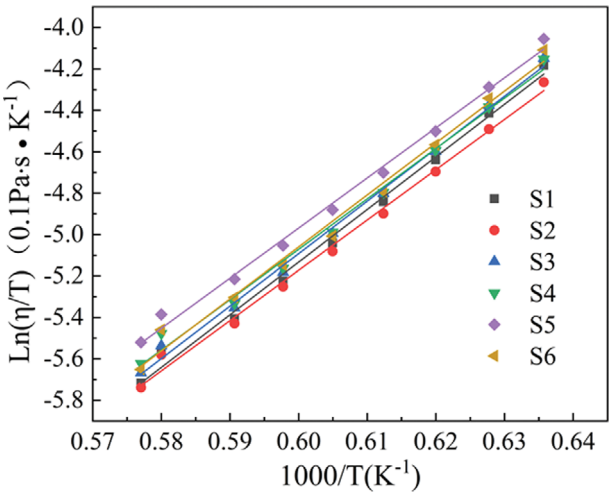

Fig. 4. Fitting curves of slope B and intercept lnA.

Table 5. Linear fitting results

Numbering	B	lnA	R^2
S1	25.57	−20.48	0.997
S2	24.54	−19.91	0.997
S3	25.24	−20.24	0.995
S4	24.50	−19.77	0.997
S5	24.89	−19.91	0.998
S6	25.84	−20.58	0.996

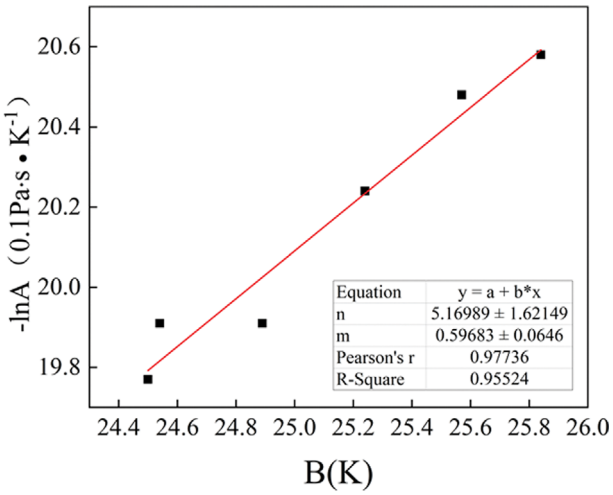

Fig. 5. m, n parametric fitting curve.

corresponding slope B and intercept lnA through linear fitting. The fitting results are shown in Fig. 4 and Table 5, and the fitting correlation coefficients R^2 are all higher than 0.995.

According to formula (2) $-\ln A = mB + n$, the −lnA and B of the six samples in Table 5 were plotted again. The slope m and the ordinate intercept n of the fitted line are obtained as shown in Fig. 5 [31], and the correlation coefficient R^2 is 0.955. From Fig. 5, we can see that the values of m and n are 0.60 and 5.17, respectively, so the formula (3) applicable to the CaO-MgO-Al_2O_3-SiO_2-Cr_2O_3 system can be determined as follows:

$$-\ln A = 0.60B + 5.17 \tag{3}$$

2. Effectiveness Analysis of the Optimized Urbain Model

2-1. Calculation of B Value in Urbain Model

After obtaining the pending constants m and n suitable for the CaO-SiO_2-MgO-Al_2O_3-Cr_2O_3 system, the viscosity of the slag (or glass) of the CaO-SiO_2-MgO-Al_2O_3-Cr_2O_3 system can be carried out. The value of viscous activation energy B in the Urbain model needs to be calculated first, and the specific calculation formula and parameters are shown in formulas (4)-(10) and Table 6 [32-34].

$$B = \frac{\sum X_M B_M}{\sum X_M} \tag{4}$$

where the molar fractions of the three types of oxides in the slag (or glass) applicable to this study (the molar fractions after the normalization of the three types of oxides) are expressed as follows (X_i is the molar fraction of the components):

$$\text{acid oxide: } X_G = X_{SiO_2} \tag{5}$$

$$\text{basic oxide: } X_M = \sum X_{M_xO} \tag{6}$$

$$\text{amphoteric oxide: } X_A = X_{Al_2O_3} \tag{7}$$

The B_M value of different basic oxides is:

$$B_M = B_0 + B_1 X_G + B_2 (X_G)^2 + B_3 (X_G)^3 \tag{8}$$

$$B_i = a_i + b_i^M \alpha + c_i^M \alpha \quad (i=0\text{-}3) \tag{9}$$

$$\alpha = \frac{\sum X_M}{\sum X_M + X_A} \tag{10}$$

The values of a_i, b_i and c_i in Urbain model are shown in Table 6.

The value of viscous activation energy B was calculated by using the parameters in formulas (4)-(10) and Table 6. The value of B was substituted into formula (3) to obtain the value of pre-exponential factor A, and then the A value and the B value were substituted into formula (1), and the viscosity value at a specific temperature can be predicted by the Urbain model.

2-2. Effectiveness Analysis of Urbain Model

To further verify the effectiveness of the optimized Urbain viscosity model, the model was used to calculate the viscosity of 66 data at 11 temperature points in the range of 1,400 to 1,500 °C under six groups of Cr_2O_3 content in this study, and the calculated values were compared with the experimented values. The comparison curves of the six groups of samples are shown in Fig. 6.

In order to verify the universality of the optimized Urbain model, according to the chemical composition of the slag of CaO-MgO-Al_2O_3-SiO_2-Cr_2O_3 system in the relevant literature (as shown in Table 7 A1 and A2) [35,36], the viscosity values of A1 and A2 were calculated by using the optimized Urbain model in this study, a total of 22 data, and compared with the experimented viscosity values in the literature. The comparison curves of A1 and A2 are shown in Fig. 7.

As can be seen from Fig. 6 and Fig. 7, there is a certain error between the experimented viscosity value and the calculated viscosity value, and the viscosity error calculation is carried out by the relative error formula (11) [37].

Table 6. Urbain model parameters

i	a_i		b_i		c_i	
	Mg	Ca	Mg	Ca	Mg	Ca
0	13.20		15.90	41.50	−18.60	−45.00
1	30.50		−54.10	−117.20	33.00	130.00
2	−40.40		138.00	232.10	−112.00	−298.60
3	60.80		−99.80	−156.40	97.60	213.60

Table 7. Composition of CaO-MgO-Al_2O_3-SiO_2-Cr_2O_3 system slag in the literature (mass fraction, %)

Numbering	CaO	MgO	Al_2O_3	SiO_2	Cr_2O_3
A1	33.33	8.20	23.20	32.67	2.00
A2	37.00	8.00	17.00	37.00	1.00

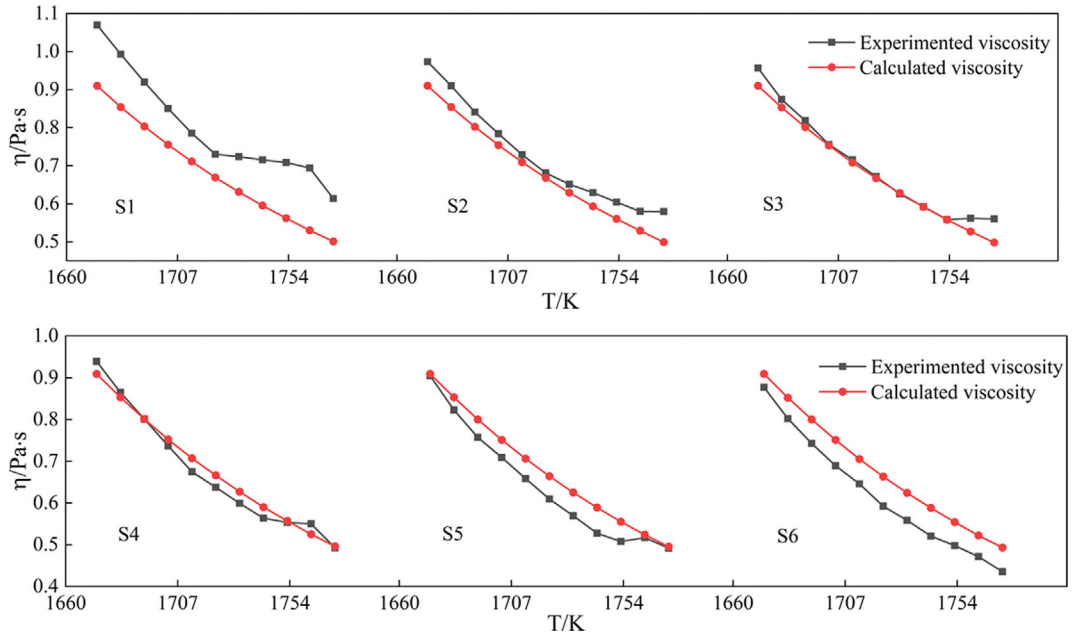

Fig. 6. Comparison of experimented viscosity and calculated viscosity of six groups of samples.

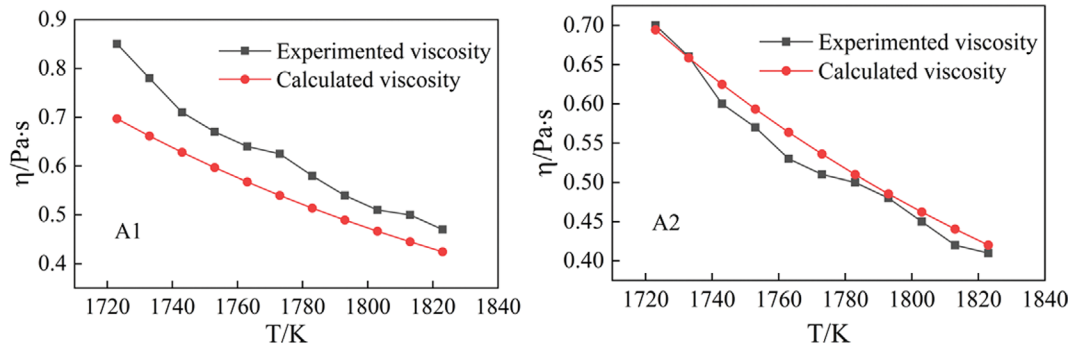

Fig. 7. Comparison of experimented viscosity and calculated viscosity of A1 and A2.

$$\Delta = \frac{1}{n} \times \sum \left| \frac{\eta_{Calc} - \eta_{Exp}}{\eta_{Exp}} \right| \times 100\% \quad (11)$$

In the formula, Δ—error,
n—the number of all experimental data,
η_{Calc}—the calculated viscosity,
η_{Exp}—the experimented viscosity.

According to the calculation, the viscosity errors of the six groups of samples in this study are 14.80%, 5.89%, 2.65%, 2.84%, 5.89% and 9.80%, respectively, and the average error is 6.98%. The viscosity errors of A1 and A2 in the literature data are 11.87% and 2.88%, respectively. In industrial production, 20% of the error is acceptable [38], indicating that the optimized Urbain model can achieve effective prediction effects, and has universality for predicting the slag (or glass) viscosity of CaO-MgO-Al_2O_3-SiO_2-Cr_2O_3 system.

3. Raman Spectroscopy Analysis of Melt Structure

The Raman spectra lines of silicate melt structure are mainly envelope lines formed by overlapping characteristic spectra peaks of various structural units. The high frequency region of Raman spectrum 800-1,200 cm^{-1} can better reflect the variation law of melt tetrahedron unit Q_n, so the high frequency region is selected as the

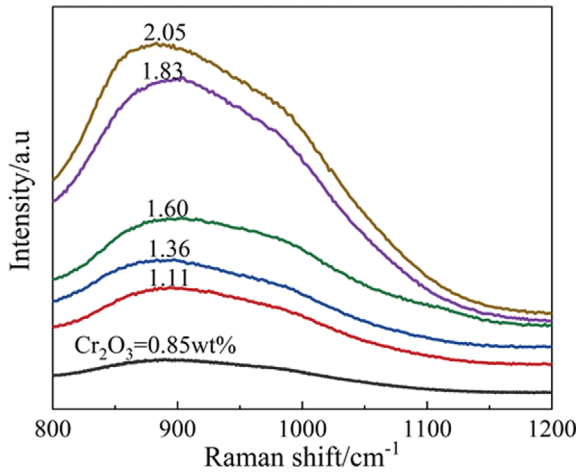

Fig. 8. Raman spectral curves of water quenched samples.

main research band [39]. Fig. 8 shows the Raman spectral envelope lines of the water quenched samples with Cr_2O_3 mass fraction of 0.85%, 1.11%, 1.36%, 1.60%, 1.83% and 2.05%, respectively, in the high frequency region.

It can be seen from Fig. 8 that when the mass fraction of Cr_2O_3 increases from 0.85% to 2.05%, the band around 890 cm^{-1} of the Raman curve gradually shifts to the left, indicating that the increase of Cr_2O_3 content causes certain changes in the structural units of silicate melt [40]. To further explore the change of melt structure, Peakfit software was used for peak splitting and fitting analysis of the envelope lines in the 800-1,200 cm^{-1} band to separate each microstructure information in Q_n, and Q_4 with weak vibration mode strength in this band that was ignored [41]. The peak splitting results of all envelope lines are shown in Fig. 9(a)-(f), where the fitting correlation coefficient $r^2 \geq 0.998$.

It can be seen from Fig. 9 that the peak positions of Q_n are all within the range of the corresponding Raman displacement region. With the increase of Cr_2O_3 content in the glass, the peak levels of Q_0 and Q_1 are significantly offset to the low band, the peak level of Q_2 does not change much, and the peak position of Q_3 shows a trend of shifting to the high band, indicating that the increase of Cr_2O_3 content results in the change of Q_n structure [42]. The area of the curve under the Q_3 peak can characterize the number of more complex silicon oxygen tetrahedrons, the change of the relative area of Q_3 (the ratio of the area of the Q_3 curve to the area of the corresponding envelope line) with Cr_2O_3 content is shown in Fig. 10 [43].

As can be seen from Fig. 10, when the mass fraction of Cr_2O_3 increases from 0.85% to 1.36%, the relative area of complex silicon oxygen tetrahedrons Q_3 is between 7%-10%, and when the mass

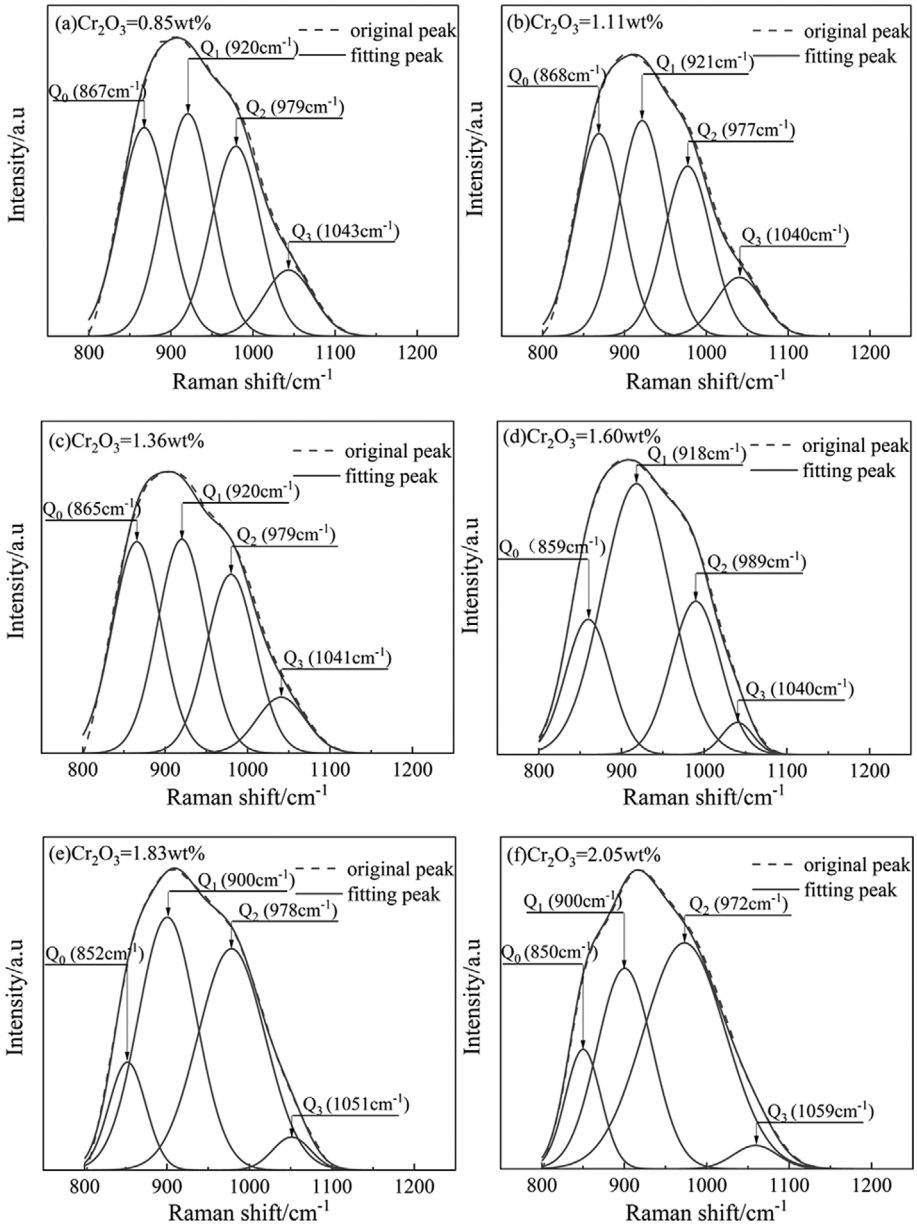

Fig. 9. (a)-(f) Envelope peaking results of water quenched samples with different Cr_2O_3 content.

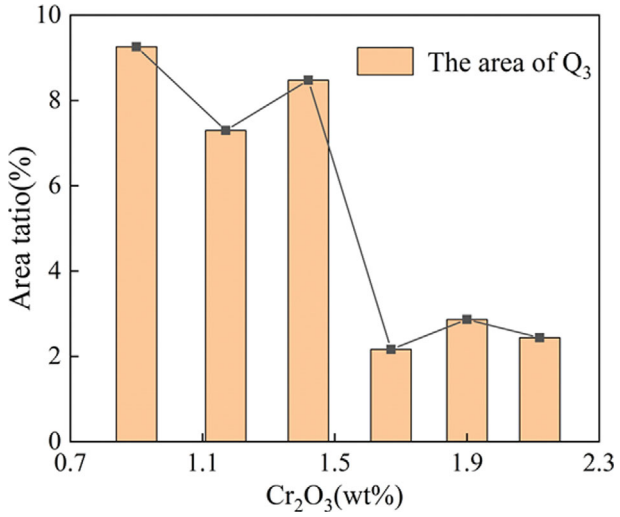

Fig. 10. The relative area of Q_3 varies with Cr_2O_3 content.

fraction of Cr_2O_3 continues to increase from 1.60% to 2.05%, the relative area of Q_3 decreases to 2%-3%. When the mass fraction of Cr_2O_3 increases from 1.36% to 1.60%, the relative area of Q_3 falls from about 9% to about 2%, which is due to the significantly enhanced effect of Cr_2O_3 as a modifier to destroy the network. The basic structural unit of SiO_2 in silicate melt is regular tetrahedral structure SiO_4^{4-}, which is connected with other tetrahedron by sharing O^{2-}. The more SiO_4^{4-} are polymerized, the more shared O^{2-} numbers are needed, and the more complex the structure of silicon-oxygen complex ions. When the mass fraction of Cr_2O_3 increases continuously, as a network modifier, Cr_2O_3 will continuously damage the network structure, dissociate the O^{2-} that connects SiO_4^{4-} to other tetrahedrons, and the silicon oxygen tetrahedrons with complex structure can be broken [44-46]. As a result, the structure of silicon-oxygen complex ions can be simplified, which is also verified by the band moving to the direction of low wave number in the Raman spectrum curve in Fig. 8 [47]. In Fig. 8, with the increase of Cr_2O_3 content, the vibration intensity of Raman spectral envelope increases gradually, indicating that the total number of silicon-oxygen complex ions increases, which is caused by the disintegration of complex silicon oxygen tetrahedrons (Q_3) into more simple silicon oxygen tetrahedrons (Q_0, Q_1, Q_2). The three-dimensional network of silicates is broken down into isolated chains, layers, and rings of ionic fluid units, resulting in sparse network structure and reduced macroscopic viscosity [48].

CONCLUSIONS

When the mass fraction of Cr_2O_3 is in the range of 0.85%-2.05%, the temperature and basicity are fixed, and the slag (or glass) viscosity of CMAS system decreases with the increase of Cr_2O_3 content. The optimized Urbain model was used to calculate the viscosity values of the six groups of samples in this study and the samples of the same system in related literatures. The error between the calculated values and the experimented viscosity values is less than 20%, which meet the requirements of industrial production, indicating that the optimized Urbain model is effective and universal for slag (or glass) of CaO-MgO-Al_2O_3-SiO_2-Cr_2O_3 system. With the increase of Cr_2O_3 content, the peak levels of Q_0 and Q_1 are significantly offset to the low band, the peak level of Q_2 does not change much, and the peak level of Q_3 shows a trend of shifting to the high band, indicating that Cr_2O_3 simplifies the Q_n structure of silicon oxygen tetrahedron melt in CMAS system. With the increase of Cr_2O_3 content, the relative area of complex silicon oxygen tetrahedrons Q_3 is reduced from 9% to 2%; in addition, the vibration intensity of the Raman spectral envelope gradually increases, indicating that the total number of silicon-oxygen complex ions in the system increases. This is due to the disintegration of complex silicon oxygen tetrahedrons (Q_3) into a larger number of simple silicon oxygen tetrahedrons (Q_0, Q_1, Q_2), resulting in sparse melt network structure and reduced macroscopic viscosity.

ACKNOWLEDGEMENTS

This work was supported by the Inner Mongolia Special Project for Transformation of Scientific and Technological Achievements [2019CG073], Solid Waste Resource National Key Research & Development Project [2020YFC1909105] and Major Science and Technology Project of Inner Mongolia Autonomous Region [2021ZD0016]. Key Project of Scientific and Technological Research in Colleges and Universities of Inner Mongolia Autonomous Region [NJZZ23056], Basic Scientific Research Business Fund Project of Universities Directly Under the Inner Mongolia Autonomous Region.

REFERENCES

1. D. Gao, F. P. Wang, Y. T. Wang and Y. N. Zeng, *Sustainability*, **12** (2020).
2. M. Rathore and A. Dalvi, *Indian J. Pure Ap. Phy.*, **51**, 372 (2013).
3. W. X. Shang, Z. W. Peng, Y. W. Huang, F. Q. Gu, J. Zhang, H. M. Tang, L. Yang, W. G. Tian, M. J. Rao, G. H. Li and T. Jiang, *J. Cleaner Production*, **317** (2021).
4. H. T. Gao, X. H. Liu, J. Q. Chen, J. L. Qi, Y. B. Wang and Z. R. Ai, *Ceram. Int.*, **44**, 6044 (2018).
5. B. E. Yekta and P. Alizadeh, *Glass Technol.*, **46**, 347 (2005).
6. W. Zhao, X. F. Huang, B. J. Yan, S. Y. Hu, H. W. Guo and D. Chen, *Sustainability-basel*, **13** (2021).
7. J. Chang, H. J. Li, K. D. Zheng, C. G. Liu, L. M. Wang, B. Li, X. N. Bu and H. Z. Shao, *Physicochem. Probl. Mi.*, **56**, 460 (2020).
8. L. B. Deng, S. Wang, Z. Zhang, Z. H. Li, R. D. Jia, F. Yun, H. Li, Y. H. Ma and W. C. Wang, *Mater. Chem. Phys.*, **251** (2020).
9. W. J. Duan, Q. B. Yu, J. X. Liu, K. Wang, H. Q. Xie, Q. Qin and Z. C. Han, *Ironmak Steelmak*, **43**, 730 (2016).
10. X. J. Dong, H. Y. Sun, X. F. She, Q. G. Xue and J. S. Wang, *Ironmak Steelmak*, **41**, 99 (2014).
11. Z. Li, Z. W. Luo, X. Y. Li, T. Y. Liu, L. M. Guan, T. Wu and A. X. Lu, *J. Porous. Mat.*, **23**, 231 (2016).
12. A. Y. Kolobov and G. A. Sycheva, *Glass Phys. Chem+*, **46**, 249 (2020).
13. W. X. Dong, Q. F. Bao, J. E. Zhou, T. G. Zhao, K. Liu, S. Z. Li, S. Y. Liu and K. X. Ma, *J. Ceram. Soc. Jpn.*, **128**, 821 (2020).
14. D. Di Genova, J. Vasseur, K. U. Hess, D. R. Neuville and D. B. Dingwell, *J. Non-cryst Solids*, **470**, 78 (2017).

15. R. Z. Xu, J. L. Zhang, Z. Y. Wang and K. X. Jiao, *Steel Res. Int.*, **88** (2017).
16. T. L. Tian, Y. Z. Zhang, H. W. Xing, J. Li and Z. Q. Zhang, *High Temp. Mat. Pr-isr*, **37**, 33 (2018).
17. I. Vilciu, *Metal Int.*, **18**, 126 (2013).
18. G. Urbain, Y. Bottinga and P. Richet, *Geochimica Et Cosmochimica Acta*, **46** (1982).
19. P. V. Riboud, Y. Roux, L. D. Lucas and H. Gaye, *Huettenprax. Metallweiterverarb*, **19**, 859 (1981).
20. K. C. Mills and S. Sridhar. *Ironmaking & Steelmaking*, **26**, 262 (1999).
21. T. Iida, H. Sakai, Y. Kita and K. Shigeno, *High Temp. Mat. Pr-isr*, **19**, 153 (2000).
22. H. Masai, *B Chem. Soc. Jpn.*, **91**, 950 (2018).
23. R. Wang and B. M. Zhang, *Spectrosc. Spectanal*, **30**, 376 (2010).
24. C. Balachandran, J. F. Munoz and T. Arnold, *Cement Concrete Res.*, **92**, 66 (2017).
25. S. Das, A. Madheshiya, S. S. Gautam and C. R. Gautam, *J. Non-Cryst. Solids*, **478**, 16 (2017).
26. Y. Shi, B. W. Li, M. Zhao and M. X. Zhang, *J. Am. Ceram. Soc.*, **101**, 3968 (2018).
27. H. Ko, M. Kim, S. M. Park and H. M. Lim, *J. Eur. Ceram. Soc.*, **58**, 160 (2021).
28. V. O. Sinelnikov and D. Kalisz, *Glass Ceram+*, **73**, 144 (2016).
29. L. Forsbacka and L. Holappa, *Scand J. Metall*, **33**, 261 (2004).
30. R. Z. Xu, J. L. Zhang, Z. Y. Wang and K. X. Jiao, *Steel Res. Int.*, **88** (2017).
31. H. S. Ray and S. Pal, *Ironmak Steelmak*, **31**, 125 (2004).
32. A. S. Kirichenko and S. M. Nekhamin, *Metallurgist+*, **64**, 548 (2020).
33. H. Y. Zheng, Y. Q. Ding, S. F. Zhou, S. F. Zhou, Q. L. Wen, X. Jiang, Q. J. Gao and F. M. Shen, *Steel Res. Int.*, **92** (2021).
34. D. Kalisz, *Arch Metall Mater*, **59**, 149 (2014).
35. R. Z. Xu, J. L. Zhang, Z. Y. Wang and K. X. Jiao, *Steel Res. Int.*, **88** (2017).
36. C. Y. Xu, C. Wang, R. Z. Xu and J. L. Zhang, *Int. J. Min. Met. Mater.*, **28**, 797 (2021).
37. T. Wu, Y. L. Zhang, F. Yuan and Z. Q. An, *Metall Mater Trans B*, **49**, 1719 (2018).
38. C. Han, M. Chen, W. D. Zhang, Z. X. Zhao, T. Evans, A. V. Nguyen and B. J. Zhao, *Steel Res. Int.*, **86**, 678 (2015).
39. H. Ko, M. Kim and S. M. Park, *J. Eur. Ceramsoc.*, **58**, 160 (2021).
40. Y. Q. Wu, G. C. Jiang and J. L. You, *J. Chem. Phys.*, **121**, 7883 (2004).
41. W. N. Li, R. Luo and C. Li, *J. Non-Cryst. Solids*, **449**, 119 (2016).
42. F. Schiavi, N. Bolfan-Casanova and A. C. Withers, *Chem. Geol.*, **483**, 312 (2018).
43. G. R Kumar and M. C. Rao, *Optik*, **181**, 721 (2019).
44. B. W. Li, L. B. Deng and X. F. Zhang, *J. Non-Cryst. Solids*, **380**, 103 (2013).
45. M. V. S. Rao, C. Rajyasree and T. Narendrudu, *Opt. Mater.*, **47**, 315 (2015).
46. S. L. Ou-Yanga, B. W. Li and X. F. Zhang, *Optoelectron Adv. Mat.*, **9** (2015).
47. A. M. Welsch, J. L. Knipping and H. Behrens, *J. Non-Cryst. Solids*, **471**, 98 (2017).
48. M. Lesniak, J. Partyka and M. Sitarz, *Phys. Chem. Glasses-B*, **58**, 1 (2017).